Eur. Phys. J. D **40**, 3–12 (2006)
DOI: 10.1140/epjd/e2006-00143-x

THE EUROPEAN PHYSICAL JOURNAL D

Long-range Rydberg-Rydberg interactions and molecular resonances

J. Stanojevic, R. Côté[a], D. Tong, S.M. Farooqi, E.E. Eyler, and P.L. Gould

Physics Department, University of Connecticut, 2152 Hillside Rd., Storrs CT 06269-3046, USA

Received 16 January 2006 / Received in final form 28 April 2006
Published online 21 June 2006 –

Abstract. We present a detailed theoretical treatment to describe the lineshape of molecular resonances in a cold dense gas of rubidium Rydberg atoms. Molecular potentials in Hund's case (c) are calculated by diagonalization of an interaction matrix. We show how the strong ℓ-mixing due to long-range Rydberg-Rydberg interactions can lead to resonances in excitation spectra. Such resonances were first reported in [S.M. Farooqi et al., Phys. Rev. Lett. **91**, 183002 (2003)], where single UV photon excitations from the $5s$ ground state occurred at energies corresponding to normally forbidden transitions or very far detuned from the atomic energies. Here, we focus our attention on resonances at energies corresponding to excited atom pairs $(n-1)p_{3/2}+(n+1)p_{3/2}$. Very good agreement between the theoretical and experimental lineshapes is found.

PACS. 32.80.Rm Multiphoton ionization and excitation to highly excited states – 32.80.Pj Optical cooling of atoms; trapping – 34.20.Cj Interatomic potentials and forces

1 Introduction

In recent years, experiments involving ultracold Rydberg gases and plasmas [1–5] have studied novel systems that are translationally cold, but with significant internal energy. The fact that highly-excited Rydberg atoms have exaggerated properties [6] is one motivation for this recent interest [7,8]. For example, in systems with one Rydberg excitation, the existence of long-range molecular bound states with very complex wave functions — the so-called "trilobite" states — have been predicted [9–13]. In addition, there have also been proposals [14] to form bound molecular states with two highly-excited atoms. Although such "macrodimers" have not yet been detected, molecular resonances caused by Rydberg-Rydberg interactions have been observed [15]. The effect of interactions between Rydberg atoms can also lead to density-dependent line broadening of resonances [16–18], and the modification of collisional processes [19]. The unique combination of properties has led to proposals to use ultracold Rydberg atoms for fast quantum gates [20,21]. Some of those schemes exploit a "dipole blockade", i.e. a strong suppression of Rydberg excitation in a confined gas, to realize elements for quantum computation between atoms [20] or in mesoscopic ensembles [21]. Recently, large inhibitions of Rydberg excitation have been observed [17,18], and a similar effect, labeled the "van der Waals blockade" has been reported [17].

[a] e-mail: rcote@phys.uconn.edu

In this paper, we present a detailed theoretical treatment to describe the lineshape of some of the molecular resonances reported in [15]. In Section 2.1, the long-range interaction potentials between Rydberg atoms are briefly described. In Sections 2.2 and 2.3, we construct a more detailed model, and show how ℓ-mixing between such long-range molecular potentials correlated to different asymptotes can give the necessary mixing of p character to allow excitation into otherwise far-off-resonance or forbidden states. The excitation lineshape is also calculated. In Section 3, we illustrate experimental evidence of such molecular resonances in an ultracold rubidium gas. The experiment uses single UV photon excitations from the $5s$ ground state to np Rydberg states ($n = 50$–90). The spectra display resonances red-detuned from the atomic resonance, at energies corresponding to excited atom pairs $(n-1)d+ns$, as well as $(n-1)p+(n+1)p$. Our theoretical lineshape is compared to the experimental result for excitations corresponding to asymptotes correlated to $(n-1)p_{3/2}+(n+1)p_{3/2}$. We particularly focus on the $69p_{3/2}+71p_{3/2}$ resonance, which has been studied in detail.

2 Theory

We start by considering the excitation of a pair of atoms, initially in the ground state, to the $np+np$ asymptote, i.e. both atoms excited into the same Rydberg state np

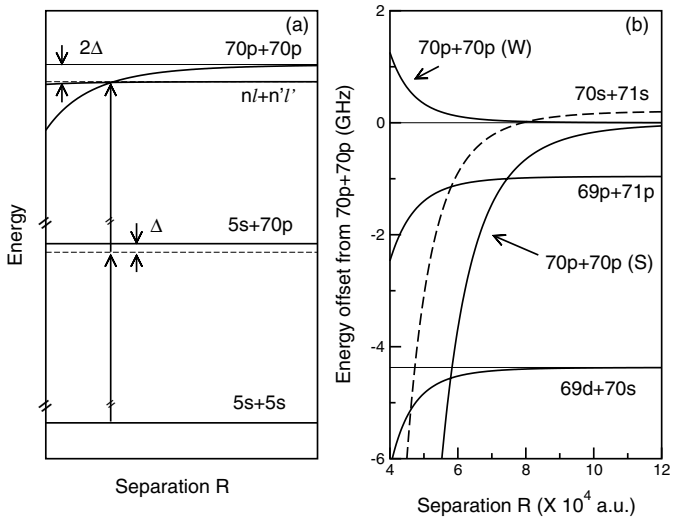

Fig. 1. (a) Two-photon excitation scheme, with detunings from the atomic resonance (Δ) and from the $70p+70p$ asymptote (2Δ), and a "curve crossing" between the states correlated to the $70p+70p$ and $n\ell+n'\ell'$ asymptotes. (b) Potential curves in Hund's case (b) in the vicinity of the $70p+70p$ asymptote for the ${}^1\Sigma_g^+$ and ${}^3\Sigma_u^+$ states.

(see the excitation scheme in Fig. 1a). We then show that well-defined resonances occur due to ℓ-mixing between $np+np$ molecular potential curves and other molecular curves sharing the same symmetries.

As will be seen below, it is remarkable that the effect of the ℓ-mixing takes place almost entirely at the energy corresponding to the $(n-1)p_{3/2}+(n+1)p_{3/2}$ asymptote, eventhough several asymptotes are involved.

To model this process, we find the molecular potential curves for a pair of atoms, and calculate the two-photon excitation probability. In Section 2.1, we discuss potential curves in Hund's case (b), where we ignore spin and ℓ-mixing between potential curves. In Section 2.2, both the spin and ℓ-mixing of various molecular states are included, and after diagonalization of the interaction matrix, the potential curves in Hund's case (c) are found; these last curves are used to calculate the excitation probability. Finally, to compare with experimental data, we obtain lineshapes and signal sizes in Section 3. Note that while one-photon transitions are far off resonance in the vicinity of molecular resonances, two-photon transitions are (nearly) resonant for most pairs; this suggests that the dominant contribution to the excitation probability comes from pair excitation. In fact, experimental results [15] show clearly that the positions of these resonances nearly coincide with the energies of a pair of isolated rubidium atoms.

2.1 Interaction potentials: Hund's case (b)

At large internuclear separations R, the interaction between two atoms can be expanded as a sum of powers of $1/R$ [22]. For two atoms in the same np state, and neglecting fine structure effects, it takes the following form [14,23]

$$V_{pp}(R) = -\frac{C_5}{R^5} - \frac{C_6}{R^6} - \frac{C_8}{R^8} - \cdots \tag{1}$$

where the C's are the dispersion coefficients. In [14], we computed the C_5, C_6, and C_8 coefficients as functions of the principal quantum number n (for Rb–Rb interactions), and found that they scale as n^8, n^{11}, and n^{15}, respectively (see also [24] for additional details). The exact values of these coefficients depend on the molecular symmetry: for the $np+np$ asymptote, a total of 12 molecular states exist, grouped in 6 pairs, each pair having the same dispersion coefficients. In Figure 1b, we illustrate two potential curves for the asymptote $70p+70p$ corresponding to ${}^1\Sigma_g^+$ and ${}^3\Sigma_u^+$ pairs of states. Notice that one pair, labeled $70p+70p$(S), has a particularly strong attractive interaction dominated by a large C_6 van der Waals coefficient (for $n=70$, $C_6 \simeq 2.64\times10^{22}$ a.u.) [14]. The other pair, labeled $70p+70p$(W), corresponds to a weaker repulsive interaction.

These potential curves may intersect potential curves correlated to nearby asymptotes, leading to avoided crossing and/or mixing between states with the same symmetry. In general, the $np+np$ potential curves can couple to curves correlated to n_1s+n_2s, n_1s+n_2d, or n_1d+n_2d through dipole interactions, and to n_1p+n_2p through quadrupole interactions. Although higher order multipoles could couple other states, the strength of such couplings decreases rapidly and hence we consider only crossings between the above states.

At large R, the leading terms of the curves for n_1s+n_2s, which are denoted as $V_{ss'}$, are

$$V_{ss'}(R) = -\frac{C_6}{R^6} - \frac{C_8}{R^8}, \tag{2}$$

while those for n_1s+n_2d or n_1p+n_2p, labeled V_{sd} and $V_{pp'}$ respectively, have the same form, namely

$$V_{sd/pp'}(R) = -\frac{C_5}{R^5} - \frac{C_6}{R^6} - \frac{C_8}{R^8}. \tag{3}$$

Finally, the leading terms for n_1d+n_2d, labeled $V_{dd'}$, are

$$V_{dd'}(R) = -\frac{C_5}{R^5} - \frac{C_6}{R^6} - \frac{C_7}{R^7}. \tag{4}$$

Naturally, the C_n coefficients are different for the various asymptotes, and depend on the particular molecular symmetries considered (see [24] for details).

Although several asymptotes corresponding to various combinations of n_1 and n_2 may lie near the $np+np$ asymptote, such as $(n-1)d+ns$ or $(n-2)d+(n+1)s$ etc., only those with small $\Delta n = |n-n_1|$ or $|n-n_2|$ have significant couplings to V_{pp}. Hence, only a few asymptotes with n_1 and n_2 near n need to be considered. In Figure 1b, we show the most important potential curves near the $70p+70p$ asymptote, namely the $69d+70s$, $69p+71p$, and $70s+71s$ asymptotes.

For some applications, the details of interactions are not crucial, and one can safely ignore effects such as fine structure coupling, ℓ-mixing, etc. For example, in the study of inhibition of Rydberg excitations due to long-range interactions [17], the interaction between atoms in $np_{3/2}$ states was described by the C_6-coefficient, assuming that all np states had the energy of the $np_{3/2}$ fine

structure component. This approximation greatly simplified the description of the excitation dynamics. In addition, the internuclear separations R between atoms were significantly greater in [17] than those considered here, so that curve crossing/mixing was not an issue. To describe strong ℓ-coupling relevant for the molecular resonances, a much more accurate description of interactions is needed. We have to diagonalize the interaction matrix to find molecular potentials and to see how states with different ℓ are coupled together.

2.2 Potentials and symmetries: Hund's case (c)

The potentials in the previous section are obtained in the second order of perturbation theory [14,24], and thus share its limitations. In addition, the effect of spin and ℓ-mixing were ignored. To describe the resonances observed in a cold dense gas of rubidium Rydberg atoms, we cannot use them directly, since the interaction energies of pairs of Rydberg atoms contributing to these resonances are many times greater than the energies for which perturbation theory is applicable. Also, formally, the C-dispersion coefficients are well defined only if fine structure is ignored, which is appropriate only if the energy separation between adjacent $n\ell+n'\ell'$ asymptotic levels is much greater then the relevant fine structure splitting. This is not true for Rydberg states of rubidium. For example, the asymptotic ($R\to\infty$) spacing between the $70s_{1/2}+71s_{1/2}$ and $70p_{3/2}+70p_{3/2}$ levels is 213 MHz, and the fine structure splitting of the $70p_{1/2}+70p_{1/2}$ and $70p_{3/2}+70p_{3/2}$ diatomic levels is 569 MHz. Depending on the energy separation, states belonging to different fine structure levels of $70p_j+70p_{j'}$ are coupled differently to the $|70s_{1/2}71s_{1/2}\rangle$ states. It turns out that the coupling between $|np_jnp_{j'}\rangle$ and $|ns_{1/2}(n+1)s_{1/2}\rangle$ states is very important for the strongly attractive $np+np$ potentials discussed in the previous section. The C_6 coefficient is almost two orders of magnitude stronger than those of other potentials. This happens because the np states lie almost exactly halfway between the adjacent ns and $(n+1)s$ states, and because of the large dipole moments between ns and np, as well as $(n+1)s$ and np states. In our discussion we focus on such strong potentials because they will mix with other potential curves as soon as they get close, resulting in avoided crossings and strong ℓ-mixing (especially the mixing of p-character which allows states with otherwise forbidden transitions to be coupled to the $5s$ ground state). Finally, an additional reason to include fine structure in our theoretical treatment is that the experiment [15] has shown that the resonances are related to certain fine structure components.

We include long-range Rydberg-Rydberg interactions $V_{\rm Ryd}(R)$ and the atomic spin-orbit interaction $H_{\rm fs}$ (which gives rise to atomic fine structure). We then diagonalize the interaction matrix,

$$U(R)=V_{\rm Ryd}(R)+H_{\rm fs}. \tag{5}$$

The eigenproblem of the interaction matrix is greatly simplified by molecular symmetry, which gives some good quantum numbers and a prescription for constructing a symmetry-adapted basis. For homonuclear diatomic molecules, the quantum numbers corresponding to the $D_{\infty h}$ point group are associated with rotations about the internuclear axis, reflections through a plane containing the rotation axis, and the inversion i of the spatial coordinates about the center point between both atom cores [25]. The projection of the total angular momentum onto the molecular axis is conserved because of the rotation symmetry. States invariant under the inversion operator i are labeled gerade (g), and those changing sign ungerade (u). Finally, the reflection operator σ_ν is used explicitly only for states with the projection of the total angular momentum equal to zero [25].

The symmetry-adapted basis for the Rydberg-Rydberg interaction $V_{\rm Ryd}(R)$ is $|^{2S+1}\Lambda_{g/u}\rangle$. Because $V_{\rm Ryd}(R)$ is essentially the residual Coulomb interaction, it is spin-independent, and cannot mix states with different Λ, S, or eigenvalues of i and σ_ν; it is diagonal in the basis $|^{2S+1}\Lambda_{g/u}\rangle|S,M_S\rangle$. However, the spin-orbit interaction $H_{\rm fs}$ depends on spin and it mixes states with different Λ; it is diagonal in the basis of properly symmetrized $|j_1,m_1\rangle|j_2,m_2\rangle$ states. We choose to represent $U(R)$ in the latter basis since it is more appropriate to describe molecular asymptotes (at $R\to\infty$), and it facilitates the calculation of lineshapes (see next section). Note that only a few molecular states with similar quantum numbers n_1 and n_2 need to be considered, because coupling is significant only for a few asymptotes nearby (see discussion below).

The projection of the total angular momentum onto the molecular axis $\Omega=m_1+m_2$ is conserved. Assuming that there is no overlap of the electronic wave functions belonging to different atoms [26], the properly symmetrized asymptotic states for $\Omega\neq 0$ have the form

$$\begin{aligned}|n\ell_j,m_j;n'\ell'_{j'},\Omega-m_j;\Omega_{g/u}\rangle\sim\\ \Big[|n,\ell,j,m_j\rangle|n',\ell',j',\Omega-m_j\rangle\\ -p(-1)^{(\ell+\ell')}|n',\ell',j',\Omega-m_j\rangle|n,\ell,j,m_j\rangle\Big].\end{aligned} \tag{6}$$

In this expression, the molecule-fixed reference frame is assumed. If $\Omega=0$, we distinguish between symmetric and antisymmetric states under σ_ν via $|0^{\pm}_{g/u}\rangle=(1\pm\sigma_\nu)/\sqrt{2}|0_{g/m}\rangle$; the action of the σ_ν operator is consistent with the following rules

$$\sigma_\nu|\Lambda\rangle=(-1)^\Lambda|-\Lambda\rangle, \tag{7}$$

$$\sigma_\nu|S,M_S\rangle=(-1)^{S-M_S}|S,-M_S\rangle. \tag{8}$$

The resonances we want to describe require strong ℓ-mixing; the strong mixing of p character corresponds to crossings with the strongly attractive $np+np$ potentials. As mentioned previously, these strong $np+np$ potentials are those coupled with $ns+(n+1)s$ states. Since Rydberg-Rydberg interactions do not mix states with

Table 1. Asymptotic 0_u^- molecular states. All of the 0_u^- states used to calculate the lineshape of the $69p+71p$ resonance are listed. The $\Omega=0$ states have to be additionally symmetrized with respect to σ_ν. Both m_j and $m_2=\Omega-m_j$ change sign under σ_ν, but the phase factors resulting from the symmetrization $(1\pm\sigma_\nu)/\sqrt{2}$ are not obvious. The result of this symmetrization is presented explicitly. We assume that all $|n\ell_j,m_j;n'\ell'_{j'},m_{j'};0_u\rangle$ states are symmetrized according to (6).

0_u^- state	Symmetrization $(1-\sigma_\nu)/\sqrt{2}\,\|0_u\rangle$
$\|70s71s,0_u^-\rangle$	$\left\{\|70s_{\frac{1}{2}},\frac{1}{2};71s_{\frac{1}{2}},-\frac{1}{2};0_u\rangle+\|70s_{\frac{1}{2}},-\frac{1}{2};71s_{\frac{1}{2}},\frac{1}{2};0_u\rangle\right\}/\sqrt{2}$
$\|70p_{\frac{3}{2}}70p_{\frac{3}{2}},0_u^-\rangle$	$\|70p_{\frac{3}{2}},\frac{3}{2};70p_{\frac{3}{2}},-\frac{3}{2};0_u\rangle$
degenerate	$\|70p_{\frac{3}{2}},\frac{1}{2};70p_{\frac{3}{2}},-\frac{1}{2};0_u\rangle$
$\|70p_{\frac{3}{2}}70p_{\frac{1}{2}},0_u^-\rangle$	$\left\{\|70p_{\frac{3}{2}},-\frac{1}{2};70p_{\frac{1}{2}},\frac{1}{2};0_u\rangle-\|70p_{\frac{3}{2}},\frac{1}{2};70p_{\frac{1}{2}},-\frac{1}{2};0_u\rangle\right\}/\sqrt{2}$
$\|70p_{\frac{1}{2}}70p_{\frac{1}{2}},0_u^-\rangle$	$\|70p_{\frac{1}{2}},\frac{1}{2};70p_{\frac{1}{2}},-\frac{1}{2};0_u\rangle$
$\|69p_{\frac{3}{2}}71p_{\frac{3}{2}},0_u^-\rangle$	$\left\{\|69p_{\frac{3}{2}},\frac{3}{2};71p_{\frac{3}{2}},-\frac{3}{2};0_u\rangle+\|69p_{\frac{3}{2}},-\frac{3}{2};71p_{\frac{3}{2}},\frac{3}{2};0_u\rangle\right\}/\sqrt{2}$
degenerate	$\left\{\|69p_{\frac{3}{2}},\frac{1}{2};71p_{\frac{3}{2}},-\frac{1}{2};0_u\rangle+\|69p_{\frac{3}{2}},-\frac{1}{2};71p_{\frac{3}{2}},\frac{1}{2};0_u\rangle\right\}/\sqrt{2}$
$\|69p_{\frac{3}{2}}71p_{\frac{1}{2}},0_u^-\rangle$	$\left\{\|69p_{\frac{3}{2}},\frac{1}{2};71p_{\frac{1}{2}},-\frac{1}{2};0_u\rangle-\|69p_{\frac{3}{2}},-\frac{1}{2};71p_{\frac{1}{2}},\frac{1}{2};0_u\rangle\right\}/\sqrt{2}$
$\|69p_{\frac{1}{2}}71p_{\frac{3}{2}},0_u^-\rangle$	$\left\{\|69p_{\frac{1}{2}},\frac{1}{2};71p_{\frac{3}{2}},-\frac{1}{2};0_u\rangle-\|69p_{\frac{1}{2}},-\frac{1}{2};71p_{\frac{3}{2}},\frac{1}{2};0_u\rangle\right\}/\sqrt{2}$
$\|69p_{\frac{1}{2}}71p_{\frac{1}{2}},0_u^-\rangle$	$\left\{\|69p_{\frac{1}{2}},\frac{1}{2};71p_{\frac{1}{2}},-\frac{1}{2};0_u\rangle+\|69p_{\frac{1}{2}},-\frac{1}{2};71p_{\frac{1}{2}},\frac{1}{2};0_u\rangle\right\}/\sqrt{2}$
$\|69s72s,0_u^-\rangle$	$\left\{\|69s_{\frac{1}{2}},\frac{1}{2};72s_{\frac{1}{2}},-\frac{1}{2};0_u\rangle+\|69s_{\frac{1}{2}},-\frac{1}{2};72s_{\frac{1}{2}},\frac{1}{2};0_u\rangle\right\}/\sqrt{2}$

different Λ, S, and eigenvalues of i and σ_ν, only configurations of the same symmetry (described by the same quantum numbers) can be coupled. By examining all possible symmetry configurations [23,24], we find that the only candidates are the asymptotically degenerate ${}^1\Sigma_g^+$ and ${}^3\Sigma_u^+$ states. After adding spin, there are three possible symmetries, 0_g^+, 0_u^- and 1_u, and only these states lead to strongly attractive potentials. Although molecular symmetries give a necessary condition for strong mixing, one has to diagonalize (5) for each symmetry individually to find which states of these molecular configurations actually give strong mixing.

The Rydberg-Rydberg interaction is conveniently expressed in the limit of large nuclear separations as an expansion in inverse powers of R. Here we consider only the first term, i.e., dipole-dipole interactions,

$$V_{\rm Ryd}(R)\simeq V_{\rm dip}(R),$$
$$=-\frac{4\pi r_1 r_2}{3R^3}\sum_{m=-1}^{1}B_2^{1+m}Y_1^m(\hat{r}_1)Y_1^{-m}(\hat{r}_2),\quad(9)$$

where $B_n^m\equiv m!/(n-m)!$ is the binomial coefficient, and $\vec{r}_i$ is the position of the electron i around its center. The goal is to calculate detailed lineshapes of $(n-1)p+(n+1)p$ resonances, particularly for $69p+71p$. These resonances are relatively close to the atomic np resonance, which means that they occur at small interaction energies and thus large internuclear separations R; in this range of R, the most important interactions are the dipole-dipole terms. Importantly, np states cannot be coupled directly via dipole-dipole interaction, and so significant ℓ-mixing is required. The matrix elements of $V_{\rm dip}(R)$ between states $|1,2\rangle\equiv|n_1,\ell_1,j_1,m_1\rangle|n_2,\ell_2,j_2,\Omega-m_1\rangle$, and $|3,4\rangle\equiv|n_3,\ell_3,j_3,m_3\rangle|n_4,\ell_4,j_4,\Omega-m_3\rangle$ can be evaluated using the following formula:

$$\langle1,2|V_{\rm dip}|3,4\rangle=$$
$$(-1)^{j_1+j_2+j_3+j_4-\Omega}\sqrt{L_1L_2L_3L_4J_1J_2J_3J_4}$$
$$\times R_{13}R_{24}\begin{pmatrix}\ell_1&1&\ell_3\\0&0&0\end{pmatrix}\begin{pmatrix}\ell_2&1&\ell_4\\0&0&0\end{pmatrix}\begin{Bmatrix}j_1&1&j_3\\\ell_3&\frac{1}{2}&\ell_1\end{Bmatrix}\begin{Bmatrix}j_2&1&j_4\\\ell_4&1/2&\ell_2\end{Bmatrix}$$
$$\times\sum_{m=-1}^{1}\begin{pmatrix}1+m\\2\end{pmatrix}\begin{pmatrix}j_1&1&j_3\\-m_1&m&m_3\end{pmatrix}\begin{pmatrix}j_2&1&j_4\\-\Omega+m_1&-m&\Omega-m_3\end{pmatrix}.\quad(10)$$

Here, $L_i=2\ell_i+1$, $J_i=2j_i+1$, and R_{13} and R_{24} are the radial parts of the dipole matrix elements of states 1, 3 and 2, 4 respectively.

To diagonalize $U(R)$, we select all states correlated with the $np+np$ and $(n-1)p+(n+1)p$ asymptotes, as well as all states correlated to the asymptotes in between. Nearby states having significant dipole-dipole couplings with these aforementioned states are also included. In the basis (6), dipole-dipole interactions give off-diagonal elements and asymptotic separations between states give diagonal terms. In the R-range considered for the $(n-1)p+(n+1)p$ resonances, the coupling due to dipole matrix elements $R_{nn'}$ decays rapidly with $\Delta n\equiv|n-n'|$; for $\Delta n=2$, it is roughly 100 times weaker than for $\Delta n=0$, and since the interaction matrix elements $\langle1,2|V_{\rm dip}|3,4,\rangle$ are quadratic in $R_{nn'}$, we neglected states corresponding to $\Delta n\geq3$. Specifically, we have included all states correlated to the following asymptotes: $ns+(n+1)s$, $np+np$, $(n-1)p+(n+1)p$ and $(n-1)s+(n+2)s$. In Table 1, we list all asymptotic states of 0_u^- symmetry used in our calculation of the $69p+71p$ resonance. The excitation probabilities are dominated by the contributions from these states.

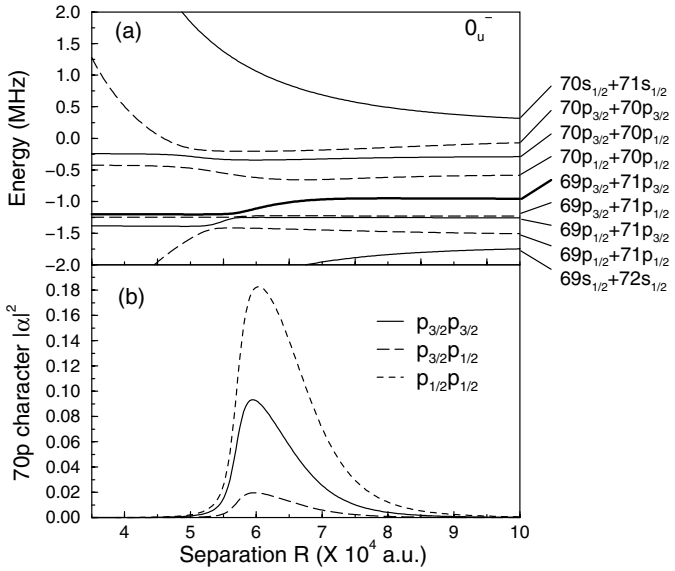

Fig. 2. (a) Potential curves for the 0_u^- symmetry corresponding to asymptotes from $70s_{1/2}+71s_{1/2}$ to $69s_{1/2}+72s_{1/2}$ centered around $69p_{3/2}+71p_{3/2}$. This latter curve is indicated by a thicker line. The zero of energy is set at the $70p_{3/2}+70p_{3/2}$ asymptote. Only curves that are not flat (within our approximations) are shown; at separation $R < 45000$ a.u., they become less reliable. (b) The fraction of $70p$ character $|\alpha|^2$ for $p_{3/2}p_{3/2}$, $p_{3/2}p_{1/2}$, and $p_{1/2}p_{1/2}$ mixtures corresponding to the potential correlated to the $69p_{3/2}+71p_{3/2}$ asymptote.

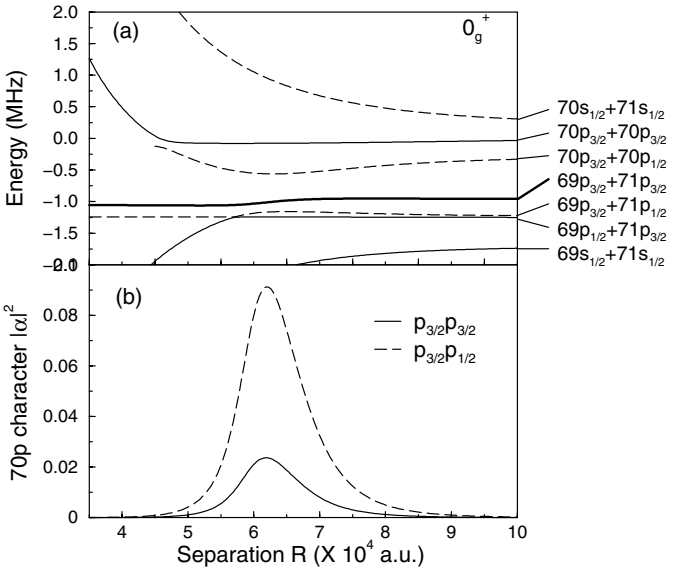

Fig. 3. Same as Figure 2 for the 0_g^+ symmetry. In (b), $|\alpha|^2$ for the $p_{1/2}p_{1/2}$ mixture is negligible and hence not shown.

In Figures 2–4, we show the potential curves for the three relevant symmetries for the resonance located near the $69p_{3/2}+71p_{3/2}$ asymptote.

2.3 Pair excitation

Here, we develop the basic theory describing the resonances observed in [15]. Although we focus our attention on resonances observed at energies corresponding to excited atom pairs $(n-1)p+(n+1)p$, the treatment given below could also be applied to the resonances corresponding the $(n-1)d+ns$ asymptotes also observed in [15]. However, because these resonances occur further below the $np+np$ asymptote, and therefore involve smaller R, many more states must be included. This case will be analyzed in a future publication.

As mentioned previously, none of these asymptotes can be excited directly by single-photon transitions from the ground $5s$ state, and since only two atomic energies are relevant for these resonances, the problem is treated essentially as a two-body effect, i.e. excitation of an interacting pair of atoms. We assume here that the sample is initially in an equal mixture of the two $|5s, j=1/2, m_j=\pm 1/2\rangle$ states, and consequently, a pair of atoms can be in any of four diatomic ground states with equal statistical probability. This means that the excitation probabilities of pairs in different initial states have to be statistically averaged. Averaging does not depend on the basis of initial states used. However, the time evolution of symmetric and antisymmetric states are independent so that choosing the basis of symmetric and antisymmetric initial diatomic states can simplify the evaluation of the excitation amplitudes. There are three symmetric initial states and one antisymmetric state. For simplicity, our notation for the $|5s, j=1/2, m_j\rangle$ ground states is $|g\, m\rangle$, where m is $\pm 1/2$. Assuming that the polarization of the optical field is along the z-axis, we have two intermediate states, depending on which fine-structure component of an np state is excited. The selection rule $\Delta m = 0$ for this laser polarization determines the polarization of the intermediate states. We label excited Rydberg states as $|e, m\rangle$ and $|e', m\rangle$, where e and e' correspond to $np_{3/2}$ and $np_{1/2}$ respectively. Here, only the calculation for the $m_1 = m_2 = \pm 1/2$ case is explained in

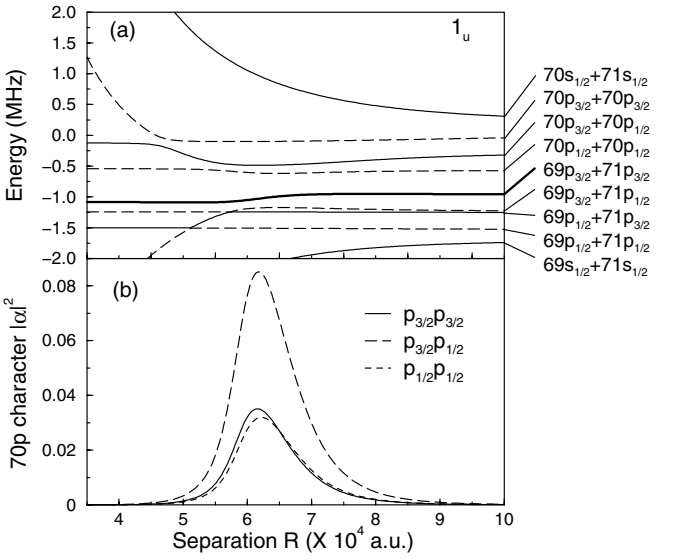

Fig. 4. Same as Figure 2 for the 1_u symmetry.

detail. The final results are given for the $m_1 = -m_2$ cases, which are evaluated in a similar fashion.

We introduce a simplified notation for diatomic states. We define $|gg\rangle \equiv |g,m\rangle|g,m\rangle$, where $m = \pm 1/2$, and similar definitions are used for $|ee\rangle$ and $|e'e'\rangle$. States $|ge\rangle$, $|ge'\rangle$ and $|ee'\rangle$ are defined as symmetric superpositions; e.g., $|ge\rangle = \{|g,m\rangle|e,m\rangle + |e,m\rangle|g,m\rangle\}/\sqrt{2}$. The doubly-excited atom pair states $|ee\rangle$, $|ee'\rangle$, and $|e'e'\rangle$ are convenient for writing the equations for the excitation amplitudes.

In our calculation, the actual doubly-excited states, labeled as $|\varphi_\lambda(R)\rangle$, correspond to the molecular potential curves $\epsilon_\lambda(R)$; they are eigenvectors and eigenvalues of (5), respectively. Many potential curves λ contribute, to various degrees, to the population of excited pairs of atoms. For example, for the curves shown in Figures 2–4, which correlate to asymptotes ranging from $70s_{\frac{1}{2}} + 71s_{\frac{1}{2}}$ down to $69s_{\frac{1}{2}} + 72s_{\frac{1}{2}}$, we included a total of 25 contributions, with $\lambda = 1$ to 9 for the 0_u^- symmetry, $\lambda = 10$ to 16 for the 0_g^+ symmetry, and $\lambda = 17$ to 25 for the 1_u symmetry. We evaluate the sum of all these contributions to find the expected signal for a given detuning from the atomic np resonance. Large populations of excited pairs of atoms occur when the two-photon energy is nearly resonant with one of the asymptotic levels, $\epsilon_\lambda(R \to \infty)$, and when $|\varphi_\lambda(R)\rangle$ has a significant np-component due to ℓ-mixing. In addition, as in standard lineshape theory (e.g., using a quasi-static treatment), a feature is expected when the first derivative of $\epsilon_\lambda(R)$ vanishes. These effects may lead to the appearance of a molecular resonance in spectra. Because the number of atom pairs with a given value of R scales as R^2 in a uniform sample, larger features are expected when these effects are satisfied at larger R.

To solve for the excitation probability, we solve the coupled time-dependent Schrödinger equation. The Hamiltonian of an interacting pair of atoms is (in the rotating frame and in the rotating-wave approximation)

$$H = \sum_{i=1}^{2} \left[\Delta\sigma_{ee}^i + \Delta'\sigma_{e'e'}^i\right] + \sum_{i=1}^{2}\left[\frac{\omega}{2}\sigma_{eg}^i + \frac{\omega'}{2}\sigma_{e'g}^i + \text{h.c.}\right] + \left[\Delta_\lambda + \epsilon_\lambda(R)\right]|\varphi_\lambda\rangle\langle\varphi_\lambda|\,, \tag{11}$$

where ω, ω', and Δ, Δ' are single-photon Rabi frequencies and detunings relative to the $np_{3/2}$ and $np_{1/2}$ fine structure components, respectively. Here Δ_λ is defined as the two-photon detuning from the asymptotic level determined by $\epsilon_\lambda(R \to \infty)$. The operators σ_{eg}^i and σ_{ee}^i are given by

$$\sigma_{eg}^i = \sum_m |e_i,m\rangle\langle g_i,m|, \tag{12}$$

$$\sigma_{ee}^i = \sum_m |e_i,m\rangle\langle e_i,m|. \tag{13}$$

Our wave function is the superposition

$$|\psi\rangle = c_0\,|gg\rangle + c_1\,|ge\rangle + + c_1'\,|ge'\rangle + c_2\,|\varphi_\lambda\rangle\,. \tag{14}$$

Solving the Schrödinger equation

$$i\frac{\partial\psi}{\partial t} = H\psi, \tag{15}$$

we obtain four equations for the excitation amplitudes $c(t)$,

$$i\frac{dc_0}{dt} = \frac{\omega^*}{\sqrt{2}}c_1 + \frac{\omega'^*}{\sqrt{2}}c_1', \tag{16}$$

$$i\frac{dc_1}{dt} = \Delta c_1 + \frac{\omega}{\sqrt{2}}c_0 + \frac{\omega^*}{\sqrt{2}}\langle ee|\varphi_\lambda\rangle c_2 + \frac{\omega'^*}{2}\langle ee'|\varphi_\lambda\rangle c_2, \tag{17}$$

$$i\frac{dc_1'}{dt} = \Delta' c_1' + \frac{\omega'}{\sqrt{2}}c_0 + \frac{\omega'^*}{\sqrt{2}}\langle e'e'|\varphi_\lambda\rangle c_2 + \frac{\omega^*}{2}\langle ee'|\varphi_\lambda\rangle c_2, \tag{18}$$

$$i\frac{dc_2}{dt} = (\Delta_\lambda + \epsilon_\lambda(R))c_2 + \frac{\omega}{\sqrt{2}}\langle\varphi_\lambda|ee\rangle c_1 + \frac{\omega'}{\sqrt{2}}\langle\varphi_\lambda|e'e'\rangle c_1' + \frac{\omega'}{2}\langle\varphi_\lambda|ee'\rangle c_1 + \frac{\omega}{2}\langle\varphi_\lambda|ee'\rangle c_1'. \tag{19}$$

For the $69p + 71p$ resonance, the one-photon detunings Δ and Δ' are large, about $2\pi \times 480$ MHz and $2\pi \times 195$ MHz from resonance, respectively, while the Rabi frequencies ω and ω' are about 250 MHz and 110 MHz, respectively (using the experimental parameters, see next section). Over the range of the experimental scan, $\Delta/2\pi = 400$–900 MHz, and we have $\Delta \gg \omega$ and $\Delta' \gg \omega'$. We can adiabatically eliminate c_1 and c_1' using equations (17) and (18), to obtain

$$c_1 \approx -\frac{\omega}{\sqrt{2}\Delta}c_0 - \left[\frac{\omega^*}{\sqrt{2}\Delta}\langle ee|\varphi_\lambda\rangle + \frac{\omega'^*}{2\Delta}\langle ee'|\varphi_\lambda\rangle\right]c_2,$$

$$c_1' \approx -\frac{\omega'}{\sqrt{2}\Delta'}c_0 - \left[\frac{\omega'^*}{\sqrt{2}\Delta'}\langle e'e'|\varphi_\lambda\rangle + \frac{\omega^*}{2\Delta'}\langle ee'|\varphi_\lambda\rangle\right]c_2.$$

Substituting these two expressions in the formulae (16) and (19) for c_0 and c_2, we formally obtain the Bloch equations of a two-level system

$$i\frac{dc_0}{dt} = -\frac{\omega_{\text{eff}}^*}{2}c_2 \tag{20}$$

$$i\frac{dc_2}{dt} = \left[\Delta_\lambda + \epsilon_\lambda(R)\right]c_2 - \frac{\omega_{\text{eff}}}{2}c_0. \tag{21}$$

The effective two-photon Rabi frequency is

$$\omega_{\text{eff}} = \frac{\omega^2}{\Delta}a_{ee}(\lambda) + \frac{\omega\,\omega'}{\sqrt{2}\frac{\Delta\,\Delta'}{\Delta+\Delta'}}a_{ee'}(\lambda) + \frac{\omega'^2}{\Delta'}a_{e'e'}(\lambda), \tag{22}$$

where $a_{ee}(\lambda) = \langle ee|\varphi_\lambda\rangle$, $a_{ee'}(\lambda) = \langle ee'|\varphi_\lambda\rangle$ and $a_{e'e'}(\lambda) = \langle e'e'|\varphi_\lambda\rangle$. We here assumed that all of the a_{ij} coefficients are real. In equations (20) and (21), we neglect all AC-Stark shifts and terms proportional to a^2. The a-coefficients measure the different p-characters in $|\varphi_\lambda(R)\rangle$. If the molecular state has no p-character at all, then $\omega_{\text{eff}} = 0$ and the transition to $|\varphi_\lambda(R)\rangle$ is forbidden. We note that the eigenstates $|\varphi_\lambda(R)\rangle$ are defined in the molecule-fixed reference frame while all other states used in the calculation are defined in the space-fixed frame (since their definitions are related to the optical

field polarization). This means that all of the projections contained in these coefficients depend on the orientation of the internuclear axis, thus the excitation probabilities have to be averaged over all possible spatial orientations of the internuclear axis. If we write $a_{ee}(\lambda) = \sum_i \langle ee|np_{\frac{3}{2}}np_{\frac{3}{2}};i\rangle\langle np_{\frac{3}{2}}np_{\frac{3}{2}};i|\varphi_\lambda\rangle \equiv \sum_i b_{ee,i}(\lambda)\alpha_{ee,i}(\lambda)$, where $|np_{\frac{3}{2}}np_{\frac{3}{2}};i\rangle$ is the ith asymptotic molecular state in the molecule-fixed frame corresponding to the appropriate symmetry, then all the angular dependence due to the two different frames is included in the $b_{ee,i}(\lambda)$ coefficient, while the $\alpha_{ee,i}(\lambda)$ coefficient describes the $np_{\frac{3}{2}}np_{\frac{3}{2}}$ character contained in the state $|\varphi_\lambda\rangle$. Similar expressions can be written for $a_{ee'}$ and $a_{e'e'}$, with projections onto the $|np_{\frac{3}{2}}np_{\frac{1}{2}};i\rangle$ and $|np_{\frac{1}{2}}np_{\frac{1}{2}};i\rangle$ states, respectively. In Figures 2–4, we show the $|\alpha|^2$ for the three symmetries, corresponding to the $70p$ characters in the potential curve correlated to the $69p_{3/2} + 71p_{3/2}$ asymptote.

We can eliminate ω' using the relation $\omega/\omega' = \sqrt{f_{3/2}/f_{1/2}}$, where $f_{3/2}$ and $f_{1/2}$ are the oscillator strengths of the $p_{3/2}$ and $p_{1/2}$ fine structure components, respectively. The ratio $f_{3/2}/f_{1/2}$ for high Rydberg states of rubidium atoms is not statistical and is approximately 5–10 [27]. We then find that $\omega_{\rm eff}(t) = \beta_1(\lambda)\omega^2(t)$, where $\beta_1(\lambda)$ is time-independent,

$$\beta_1(\lambda) = \left(\frac{a_{ee}(\lambda)}{\Delta} + \sqrt{\frac{f_{1/2}}{2f_{3/2}}}\frac{\Delta+\Delta'}{\Delta\Delta'}a_{ee'}(\lambda) + \frac{f_{1/2}/f_{3/2}}{\Delta'}a_{e'e'}(\lambda)\right). \quad (23)$$

If we perform the phase transformation $c_2 \equiv \exp[-i(\Delta_\lambda + \epsilon_\lambda(R))t]\bar{c}_2$, our Bloch equations take the simpler form

$$i\frac{dc_0}{dt} = -\frac{\omega^*_{\rm eff}}{2}e^{-i(\Delta_\lambda+\epsilon_\lambda(R))t}\bar{c}_2, \quad (24)$$

$$i\frac{d\bar{c}_2}{dt} = -\frac{\omega_{\rm eff}}{2}e^{i(\Delta_\lambda+\epsilon_\lambda(R))t}c_0. \quad (25)$$

The processes considered are far from (atomic) resonance. This means that $c_0 \approx 1$. Using this approximation and $\omega_{\rm eff}(t) = \beta_1(\lambda)\omega^2(t)$, we get our final formula for $\bar{c}_2$,

$$\bar{c}_2(t\to\infty) = -\frac{i\,\beta_1(\lambda)}{2}\int_\infty^{-\infty}\omega^2(t')e^{i(\Delta_\lambda+\epsilon_m(R))t'}dt' = -i\,\beta_1(\lambda)\sqrt{\pi/2}\,F_{(\Delta_\varphi+\epsilon_\lambda(R))}[\omega^2(t')], \quad (26)$$

where $F_\nu[h(t)]$ is the Fourier transform of $h(t)$ with respect to ν. Although the Fourier transform of $\omega^2(t)$ is not equal to the Fourier transform of the optical field, they are related. The probability $P_1(\lambda)$ to excite the doubly-excited state $|\varphi_\lambda(R)\rangle$ is

$$P_1(\lambda) = {\rm Abs}\left[\bar{c}_2^2(t\to\infty)\right], = \frac{\beta_1^2(\lambda)\pi}{2}{\rm Abs}\left[F^2_{(\Delta_\lambda+\epsilon_\lambda(R))}(\omega^2(t))\right]. \quad (27)$$

The previous analysis assumed that $m_1 = m_2$ for a pair of atoms in the ground state. We now consider the situation where $m_1 = -m_2$. In this case, we can construct symmetric and antisymmetric combinations

$$|\widetilde{gg}\rangle = \frac{1}{\sqrt{2}}\left\{|g,m\rangle\,|g,-m\rangle + q\,|g,-m\rangle\,|g,m\rangle\right\}, \quad (28)$$

$$|\widetilde{ee}\rangle = \frac{1}{\sqrt{2}}\left\{|e,m\rangle\,|e,-m\rangle + q\,|e,-m\rangle\,|e,m\rangle\right\}, \quad (29)$$

$$|\widetilde{ee'}\rangle = \frac{1}{\sqrt{2}}\left\{|e,m\rangle\,|e',-m\rangle + q\,|e',-m\rangle\,|e,m\rangle\right\}, \quad (30)$$

$$|\widetilde{e'e}\rangle = \frac{1}{\sqrt{2}}\left\{|e',m\rangle\,|e,-m\rangle + q\,|e,-m\rangle\,|e',m\rangle\right\}, \quad (31)$$

where $q = 1(-1)$ for symmetric(antisymmetric) states. The a-coefficients in this case are defined as follows $\tilde{a}_{ee}(\lambda) = \langle\widetilde{ee}|\varphi_\lambda\rangle$, $\tilde{a}_{ee'}(\lambda) = \langle\widetilde{ee'}|\varphi_\lambda\rangle$, $\tilde{a}_{e'e}(\lambda) = \langle\widetilde{e'e}|\varphi_\lambda\rangle$, and $\tilde{a}_{e'e'}(\lambda) = \langle\widetilde{e'e'}|\varphi_\lambda\rangle$. We obtain an expression very similar to the previous one for the excitation probability of doubly-excited states, $|\varphi_\lambda(R)\rangle$

$$P_2(\lambda) = \frac{\beta_2^2(\lambda)\pi}{2}{\rm Abs}\left[F^2_{(\Delta_\lambda+\epsilon_\lambda(R))}(\omega^2(t))\right], \quad (32)$$

where β_2 is given by

$$\beta_2(\lambda) = \left(\frac{\tilde{a}_{ee}(\lambda)}{\Delta} + \frac{f_{1/2}/f_{3/2}}{\Delta'}\tilde{a}_{e'e'}(\lambda) + \sqrt{\frac{f_{1/2}}{f_{3/2}}}\frac{\Delta+\Delta'}{2\Delta\Delta'}[\tilde{a}_{ee'}(\lambda)+\tilde{a}_{e'e}(\lambda)]\right). \quad (33)$$

To calculate the lineshape in the vicinity of a molecular resonance, P_1 and P_2 are averaged over initial diatomic states and all possible orientations of the internuclear axis, which gives $\langle\beta^2\rangle$. Finally, we sum the pair excitation probabilities of different doubly-excited states $|\varphi_\lambda(R)\rangle$ to get the average excitation probability of a pair of atoms at internuclear separation R. The excitation probability per atom is the sum of all excitation probabilities of pairs that include a given atom,

$$P_{\rm exc} = \sum_\lambda 2\pi^2\int_0^\infty dR\,R^2\rho\,\langle\beta^2(\lambda)\rangle \times {\rm Abs}\left[F^2_{(\Delta_\lambda+\epsilon_\lambda(R))}(\omega^2(t))\right], \quad (34)$$

where ρ is the sample density. Figures 2–4 illustrate the relevant α-coefficients for the signal corresponding to the $69p+71p$ resonance. Although the relative phase between them is important, their square is plotted. Note that all averaging over angles is included in $\langle\beta^2\rangle$.

For a Gaussian pulse of duration τ (FWHM) and bandwidth Γ (FWHM), the Fourier transform of ω^2 is given by (with $\epsilon_\lambda(R)$ and Δ_λ in angular frequencies)

$${\rm Abs}\left[F^2_{(\Delta_\lambda+\epsilon_\lambda(R))}(\omega^2(t))\right] = 2^{-[\Delta_\lambda+\epsilon_\lambda(R)]^2/2\pi^2\Gamma^2}\frac{I^2}{I^2_{\rm sat}}\frac{\pi\ln^2 2}{\tau^3\Gamma}. \quad (35)$$

This formula shows the expected quadratic dependence on the laser intensity I. We do not assume in equation (35)

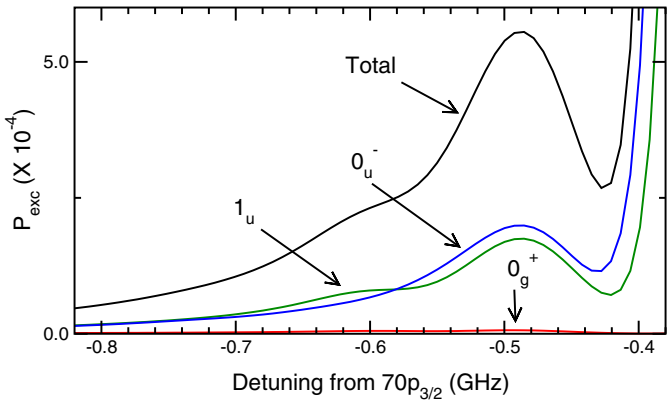

Fig. 5. Convolutions for the three symmetries and the total lineshape, in the vicinity of the $69p_{3/2} + 71p_{3/2}$ asymptote, using $I/I_{\rm sat} = 0.354$ and a density of 6×10^{10} cm^{-3}. The total lineshape includes twice the contribution of 1_u since that state is twice degenerate (as opposed to 0_g^+ and 0_u^-). The horizontal-axis is the single-photon detuning from the $70p_{3/2}$ atomic resonance.

that Γ is equal to the Fourier transform limit, but the saturation intensity $I_{\rm sat}$ for isolated $np_{3/2}$ atoms is defined using this ideal pulse.

Figure 5 shows $P_{\rm exc}$ in the vicinity of the $69p_{3/2} + 71p_{3/2}$ energy. The contributions of the three symmetries and the resulting lineshape are plotted in terms of the single-photon detuning from the $70p_{3/2}$ atomic resonance.

3 Experiment and discussion

The experimental approach is similar to photoassociative spectroscopy in ultracold samples [28,29], where two colliding atoms interact with laser light resonant with a transition from the initial continuum ground state to an excited bound state of the molecule. This technique has been used extensively to investigate the long-range molecular potentials associated with low-lying excited atomic states. The experiment described here differs in two respects from most photoassociative spectroscopy: the principal quantum numbers are much higher, and the molecular resonance is a two-photon excitation, in which both of the interacting atoms are excited simultaneously (see previous section).

3.1 Experimental set-up

In the experiment, an ultracold sample of ^{85}Rb atoms is provided by a vapor-cell magneto-optical trap (MOT) with a typical peak density of 10^{11} cm^{-3} at a temperature of $\sim$100 μK (see [15] for details). Intense pulsed UV laser light excites atoms in the $5s$ ($F = 3$) level to np Rydberg states. The laser delivers pulses with energies up to 1 mJ focused to a diameter 50–100 μm in the MOT cloud, yielding a cylindrical excitation volume about $\sim$1 mm long. These UV pulses of $\sim$5 ns duration are nearly transform limited ($\sim$120 MHz bandwidth). During that timescale, the ultracold atoms are essentially static, moving less than 1 nm, so that their motion can be neglected.

Subsequently ($\sim$300 ns after the UV pulses), Rydberg atoms are detected via pulsed field ionization; a short ($\sim$80 ns) high voltage pulse provides a field of $\sim$1000 V/cm that ionizes any Rydberg states above $n \sim 28$. The resulting atomic ions are detected by a microchannel plate (MCP). A pair of wire meshes surrounds the cold sample, allowing both the extraction of ions produced by pulsed field ionization and the careful nulling of stray fields [15]. Our detected signal includes atomic ions resulting from any process leading to ionization, including both bound and unbound molecular resonances, since acceleration on an attractive molecular potential can lead to short-range ionization.

Lineshapes are measured by scanning the laser frequency in the vicinity of resonances to atomic np states. By varying the detuning Δ from the atomic level np, features are observed at positions where no atomic excitation should be allowed. In the following section, we examine a resonance near the average energy of the $(n-1)p$ and $(n+1)p$ atomic states. This feature lies just below the np transition energy, although transitions to $(n-1)p$ and $(n+1)p$ are off-resonance by $\sim$21 GHz for $n = 70$.

3.2 Results and comparison with theoretical lineshapes

In Figure 6, we show a laser scan in the vicinity of the $70p$ atomic resonance. A significant broadening of the main np atomic resonances, predominantly to the red, is consistent with strong attractive Rydberg-Rydberg interactions. Both the $70p_{3/2}$ and $70p_{1/2}$ lines are visible, separated by the 285 MHz fine structure splitting, and despite possible saturation, their relative sizes illustrate the expected non-statistical $f_{3/2}/f_{1/2}$ for high Rydberg states of rubidium atoms. On this scan, a molecular resonance is seen as a small peak in the ion signal about 480 MHz to the red of the $70p_{3/2}$ line, its position being near the average energy of Rydberg atoms in the $69p_{3/2}$ and $71p_{3/2}$ states. Other apparent features, with linewidths less than that of the laser, do not reproduce from scan to scan and are attributed to experimental fluctuations. In [15], we showed that the signal size varies quadratically with the laser intensity, as predicted for a molecular resonance. Similar scans were obtained for other values of n over the range 50–70 [15].

In Figure 6, we also compare the experimental and theoretical lineshapes for the $69p_{3/2} + 71p_{3/2}$ resonance. The theoretical curve was computed using the experimental parameters: for $5s \rightarrow 70p_{3/2}$, the saturation irradiance $I_{\rm sat}$ (defined by $\omega\tau = \sqrt{2\pi \ln 2}$) is about 1.5×10^7 W/cm^2, the irradiance is $I/I_{\rm sat} \sim 0.354$, the pulse duration is 5 ns, and the bandwidth Γ (FWHM) is 120 MHz. The peak MOT density used was 6×10^{10} cm^{-3}. The theoretical curve shown in Figure 6 has been scaled to match the experimental data, and a global background (corresponding to $\sim$20% of the peak of the resonance) has been added to it. Finally, it was shifted by 35 MHz to the blue

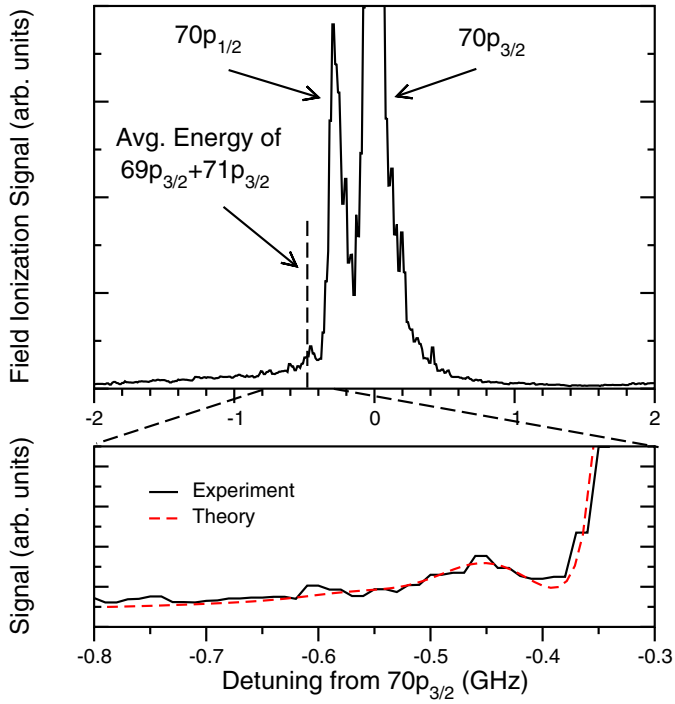

Fig. 6. (a) Experimental Rydberg spectrum near the molecular resonance red-detuned from the $70p$ atomic resonance. Both $70p_{1/2}$ and $70p_{3/2}$ fine structure components are shown. The resonance position roughly coincides with the average energy of the $69p_{3/2} + 71p_{3/2}$ asymptote. (b) Comparison of the experimental (solid line) and theoretical (dashed line). The theoretical spectrum has been shifted by 35 MHz (roughly one standard deviation) to the blue and the theoretical lineshape assumes a 120 MHz laser bandwidth.

(within the experimental uncertainty). We find good overall agreement, although there are obvious differences in the details. In both cases, we observe a slight red-detuned wing in the molecular resonance. The lineshape for the broad red wing of the main atomic resonance is also well modeled by the theoretical lineshape, implying that our theoretical values of the potential curves describe the interaction reasonably well. Regarding the absolute signal size, uncertainties in the experimental parameters, such as ion detector response, laser intensity, and atomic density, prevent a precise comparison with theory. Possible detector saturation and blockading of atomic excitation [17,18] are further complications. Nevertheless, the calculated and measured signals are in reasonable agreement, although the calculated signal of ∼300 ions per shot (using the experimental parameters) is smaller by a factor 5–10. Note that the position of the theoretical signal is located only 5–6 MHz to the red of the average energy of the atom pair $69p_{3/2} + 71p_{3/2}$.

It is remarkable that the effect of the ℓ-mixing takes place almost entirely at the energy corresponding to the $(n-1)p_{3/2} + (n+1)p_{3/2}$ asymptote, even-though several asymptotes are involved. It is in part due to the non-statistical $f_{3/2}/f_{1/2}$ ratio. In addition, from Figures 2–4, we find that the $|\alpha|^2$ $70p$-characters peak around $R_0 \sim 62\,000a_0$ (a_0: bohr radius), with $\Delta R \sim 15\,000a_0$ (chosen as the FWHM of $|\alpha|^2$). The $|\alpha|^2$ $70p$-character for the other potential curves also exhibits maxima in the same range, but are much smaller, hence their weaker contribution to the total lineshape.

4 Conclusion

We have presented a theoretical treatment predicting molecular resonances due to avoided crossing and ℓ-mixings between long-range potential curves of pairs of excited Rydberg atoms. Expressions are given for the lineshape of these resonances, as well as the scaling of the signal as a function of n. The calculated lineshape for the $69p_{3/2} + 71p_{3/2}$ resonance compares well with experimental observations.

Many other such avoided crossings and ℓ-mixings should give spectral features, and their detection will help in describing the long-range interaction between Rydberg atoms, and possibly lead to the detection of molecular bound levels with ultra-long equilibrium separations, the so-called "macrodimers" [14].

The authors thank T. Gallagher for pointing out the importance of the long-range dipole-dipole interactions. This work was supported in part by the the National Science Foundation. The work of R.C. was partially supported by the Department of Energy, Office of Basic Energy Sciences.

References

1. T.C. Killian et al., Phys. Rev. Lett. **83**, 4776 (1999)
2. S.K. Dutta et al., Phys. Rev. Lett. **86**, 3993 (2001)
3. M.P. Robinson et al., Phys. Rev. Lett. **85**, 4466 (2000)
4. W.R. Anderson, J.R. Veale, T.F. Gallagher, Phys. Rev. Lett. **80**, 249 (1998)
5. I. Mourachko, D. Comparat, F. de Tomasi, A. Fioretti, P. Nosbaum, V.M. Akulin, P. Pillet, Phys. Rev. Lett. **80**, 253 (1998)
6. T.F. Gallagher, *Rydberg Atoms* (Cambridge University Press, Cambridge, 1994)
7. See the Special Issue on Rydberg Physics, J. Phys. B **38** (2005) and references therein
8. See this Special Issue of Eur. Phys. J. D
9. C.H. Greene, A.S. Dickinson, H.R. Sadeghpour, Phys. Rev. Lett. **85**, 2458 (2000)
10. B.E. Granger, E.L. Hamilton, C.H. Greene, Phys. Rev. A **64**, 042508 (2001)
11. E.L. Hamilton, C.H. Greene, H.R. Sadeghpour, J. Phys. B **35**, L199 (2002)
12. M.I. Chibisov, A.A. Khuskivadze, I.I. Fabrikant, Phys. Rev. A **66**, 042709 (2002)
13. A.A. Khuskivadze, M.I. Chibisov, I.I. Fabrikant, J. Phys. B **35**, L193 (2002)
14. C. Boisseau, I. Simbotin, R. Côté, Phys. Rev. Lett. **88**, 133004 (2002)
15. S.M. Farooqi, D. Tong, S. Krishnan, J. Stanojevic, Y.P. Zhang, J.R. Ensher, A.S. Estrin, C. Boisseau, R. Côté, E.E. Eyler, P.L. Gould, Phys. Rev. Lett. **91**, 183002 (2003)

16. J.M. Raimond, G. Vitrant, S. Haroche, J. Phys. B **14**, L655 (1981)
17. D. Tong, S.M. Farooqi, J. Stanojevic, S. Krishnan, Y.P. Zhang, R. Côté, E.E. Eyler, P.L. Gould, Phys. Rev. Lett. **93**, 063001 (2004)
18. K. Singer, M. Reetz-Lamour, T. Amthor, L.G. Marcassa, M. Weidemüller, Phys. Rev. Lett. **93**, 163001 (2004)
19. A.L. Oliveira, M.W. Mancini, V.S. Bagnato, L.G. Marcassa, Phys. Rev. Lett. **30**, 143002 (2003)
20. D. Jaksch, J.I. Cirac, P. Zoller, S.L. Rolston, R. Côté, M.D. Lukin, Phys. Rev. Lett. **85**, 2208 (2000)
21. M.D. Lukin, M. Fleischhauer, R. Côté, L.M. Duan, D. Jaksch, J.I. Cirac, P. Zoller, Phys. Rev. Lett. **87**, 037901 (2001)
22. A. Dalgarno, W.D. Davison, Adv. Mol. Phys. **2**, 1 (1966)
23. M. Marinescu, Phys. Rev. A **56**, 4764 (1997)
24. K. Singer, J. Stanojevic, M. Weidemüller, R. Côté, J. Phys. B **38**, S295 (2005)
25. J.M. Brown, A. Carrington, *Rotation Spectroscopy of Diatomic Molecules* (Cambridge University Press, Cambridge, 2003)
26. If the electronic wave functions overlap, the same expression with the prime and unprimed labels interchanged would be added
27. J. Migdalek, Y.-K. Kim, J. Phys. B **31**, 1947 (1998)
28. J. Weiner, V.S. Bagnato, S. Zilio, P.S. Julienne, Rev. Mod. Phys. **71**, 1 (1999)
29. W.C. Stwalley, H. Wang, J. Mol. Spectrosc. **195**, 236 (1999)